Analysis of switching, degradation and failure mechanisms by RTN signals in non-filamentary (a-VMCO) RRAM devices

W. Zhang, Z. Chai, J. Ma, J. F. Zhang
Department of Electronics and Electrical Engineering, Liverpool John Moores University, Liverpool L3 3AF, UK
Corresponding author, email: w.zhang@ljmu.ac.uk

Abstract

The switching, degradation and failure mechanisms in amorphous-Si/TiO_2 based non-filamentary (a-VMCO) RRAM device has been analyzed through a combination of random-telegraph-noise (RTN) and constant-voltage-stress (CVS). The pre-existing and generated defects and their impacts have been identified. The amplitude of RTN, which leads to read instability, is evaluated statistically at different stages of cell degradation and correlated with different defects. It is found that the switching between low and high resistance states (LRS and HRS) are correlated with the profile modulation of pre-existing defects in the 'defect-less' region near the a-Si/TiO2 interface. The RTN amplitude observed at this stage is small and has a tight distribution. At longer stress times, a percolation path is formed due to defects generation, which introduces larger RTN amplitude and a significant tail in its distribution.

1. Introduction

Resistive switching memory devices have attracted numerous attentions in the past decade and are considered as a strong candidate for next generations emerging memory technology [1-2]. There are mainly two types of transition-metal- oxide (TMO) based resistive switching devices (RRAM), the filamentary ones that can be made from a number of different materials, for example, HfO2 [2], etc.; and the non-filamentary ones such as a-VMCO [3].

In filament-based VCM devices, variable resistance is induced by repeatable rupture and restoration of a conductive filament (CF) of nanometer scale. The large tail in read current distribution at high resistance state (HRS) is still a major concern, as it deteriorates the resistive switching window and causes endurance and retention problems. This has been attributed to defects moving into/out of the constriction, where the least number of defects exist. The movement of individual defect to/from the constriction has significant impact on the overall resistance, and the stochastic nature of individual defect movement causes large resistance variability and large read instability [4]. Novel non-filamentary RRAM devices have been proposed recently in hope to overcome the above problems, in which the resistance switching is controlled through the uniform modulation of the defect profile [3]. Significant improvement in variability has been observed and attributed to the non-filamentary switching mechanism. The a-VMCO RRAM device consists of two layers, with TiO_2 as the switching layer and amorphous-Si as the barrier layer. It shows the non-filamentary switching behavior as its resistance is inversely proportional to the area. The resistance distributions at both HRS and LRS in a-VMCO RRAM show little tail-bits shifting [3, 5].

The switching, degradation and failure mechanisms in non-filamentary a-VMCO cells and their correlation with the switching operation and reliability will be investigated in this work, with the focus on the defects and their impact on resistance switching (LRS/HRS) and stress-induced RTN distribution. Defects profiles are extracted during different stages of CVS based on the RTN technique. Statistical analysis is carried out to characterize the RTN amplitude distribution.

2. Devices and Experiments

The a-VMCO device structure as shown in **Fig. 1b** was fabricated with CMOS-compatible process [3, 6]. The active stack is formed by an 8-nm PVD amorphous silicon (a-Si) barrier layer and, on top of which, an 8-nm ALD TiO_2 switching layer crystallized in anatase phase. The a-Si barrier layer controls the current through the stack, and it also acts as a scavenger to introduce an oxygen vacancy (Vo) profile in the TiO_2 switching layer. The stack is sandwiched by a TiN bottom electrode (BE) and a TiN top electrode (TE). The typical DC I-V characteristics is shown in **Fig. 1a**, with the external bias applied on TE, and BE grounded. A ~10× window can be achieved, showing a gradual RESET/SET process without a current compliance.

3. Results and discussions

3.1 RTN signals in aVMCO RRAM

In order to investigate the defects and their impact on resistive switching operation, RTN measurements are carried out at incremental biases for both LRS and HRS. The typical RTN measurement procedure and results are given in Fig. 3 [5-7]. Defect's location is extracted from

the dependence of RTN's mean time constants on bias VTE, based on the method adopted from refs [8-9]. Defects can be found in both TiO_2 and a-Si. RTN measurements are also inserted during the CVS stress to extract the defects induced by the stress. RTN amplitude distribution is analyzed and evaluated statistically in both fresh and degraded devices.

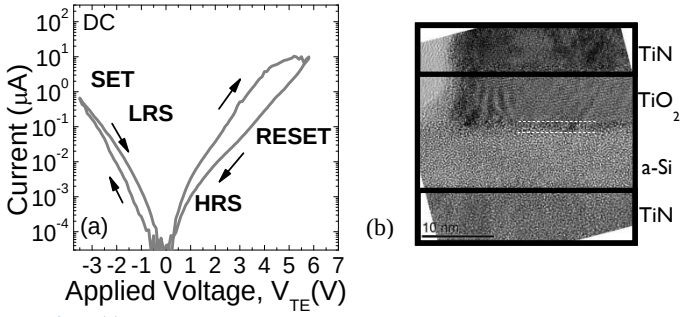

Fig.1 (a) Typical I-V characteristics during the DC RESET and SET resistive switching. (b) TEM cross-section of a smallest size (40nm) device. 1-nm SiOx interfacial layer (IL) is naturally formed between amorphous Si and anatase-phase TiO_2 by the end of the process.

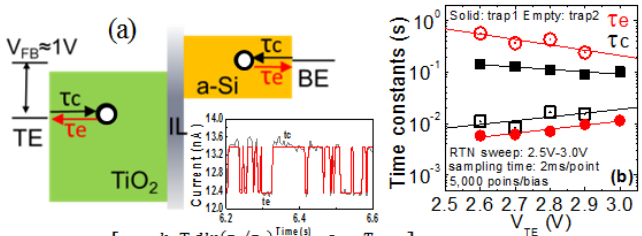

$$X_T = \left[1 - \frac{k_B T}{q}\frac{d\ln(\tau_c/\tau_e)}{dV}\left(1 + \frac{\varepsilon_{oxS}}{\varepsilon_{oxB}}\frac{T_{oxB}}{T_{oxS}}\right)\right]T_{oxS} + T_{oxB} \quad \text{(Eq.1)}$$

$$X_T = -\frac{k_B T}{q}\frac{d\ln(\tau_c/\tau_e)}{dV}\left(T_{oxB} + \frac{\varepsilon_{oxB}}{\varepsilon_{oxS}}T_{oxS}\right)T_{oxS} \quad \text{(Eq.2)}$$

Fig. 2 Typical RTN measurement procedure and results. (a) Energy band diagram and defect location measured from RTN. (b) Defect locations in TiO2 (eq.1) and a-Si (Eq.2) are extracted from the dependence of RTN's mean time constants on bias VTE by using the method adopted from refs [5-9]. Defects can be found in both TiO_2 and a-Si. RTN measurement bias, negative: -0.5V~-2V; positive: +2.0~3.0V. The mean time constants for high (τhigh) and low (τlow) current levels in RTN are the capture (τc) and emission times (τe), respectively, extracted by using the HMM method [5].

3.2 Defect Profile in aVMCO RRAM

Defects profiles are extracted at both HRS and LRS from the RTN signals in an unstressed a-VMCO device, as shown in Fig.3a. Defects exist in both TiO_2 and a-Si layers. At HRS, there is defects-'less' region at TiO_2 side of TiO_2/a-Si interfacial layer (IL), which does not exist at LRS, suggesting that defect profile modulation occurs predominantly at TiO_2 side of IL. Fig. 3b shows that the resistance states, represented by the read out current at V_{TE}=3V, are correlated well with the 'defects-less' region, as it becomes wider at HRS and narrower at LRS as illustrated in Fig.3c, confirming that the defect profile modulation in TiO_2 near the IL is responsible for the resistive switching,. This result provides direct experimental evidence for the proposed switching mechanism [2]. Note that this defect profile modulation is caused by the movement of pre-existing defects, which have uniform spatial distribution in the lateral direction. This is supported by the forming-free and area-dependent non-filamentary switching characteristics as shown in refs [3, 6].

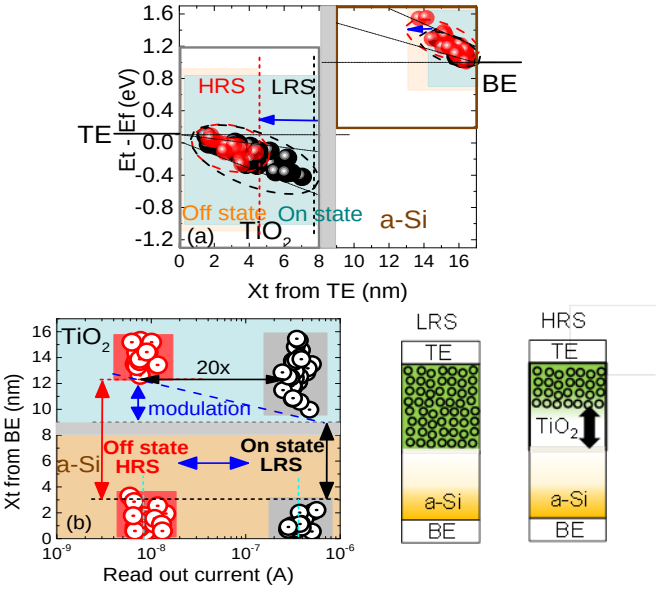

Fig.3 Extracted defects profile at LRS ('●') and HRS ('●'). (a) the distribution of extracted defects in space (from TE) is plotted vs its energy level, and (b) vs resistance state by plotting X_T (from BE) vs. I_{read} measured at V_{TE}=3.0 V during the RTN measurement sweep. Defect profile modulation predominantly occurs in a defect-'less' region in TiO_2 near IL. (c) 'Defect-less' region becomes wider at HRS, resulting in higher resistance Note that this defect profile does not provide information on the actual defect density, as explained in detail in ref. [5].

To investigate the impact of defect profile modulation on device operation, the statistical distribution of the relative amplitude of RTN signals in unstressed a-VMCO cells is further examined, as large RTN amplitude could lead to large noise during the read operation, and reduce the resistance window. As shown in Fig. 4a, RTN amplitude at LRS is relatively small, with a median value of ~4%, and a relatively tight distribution with a maximum value of ~8%. At HRS, the median increases to ~8% and the distribution is shifted almost in parallel except the lower 10% percentiles. In comparison, RTN amplitude distribution in filamentary RRAM, such as in HfO2 based RRAM devices in Fig. 4b [2, 5], is significantly different, especially at HRS. Its RTN at LRS is much smaller and tightly distributed, while at HRS the distribution is much wider with a long tail at larger relative RTN amplitudes reaching 50%.

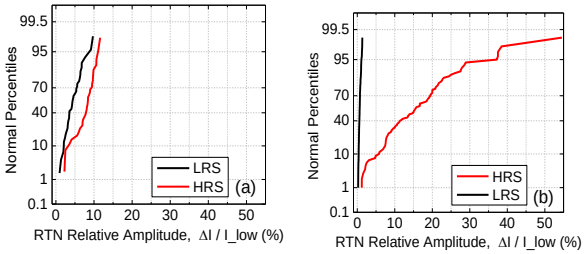

Fig. 4 Statistical distribution of the relative RTN amplitude at LRS and HRS under typical operation conditions in (a) non-filamentary a-VMCO RRAM device (Vread=3V, no compliance current is applied) and (b) HfO_2 based filamentary RRAM device with TiN/Hf(10nm)/HfO_2(5nm)/ TiN structure [3]. (Vread= 0.1V, Vbias=0.1V~0.3V, Icc=100μA). Cycle- to-cycle variability is considered in both (a) and (b).

The above differences in RTN amplitude distribution is consistent with their different HRS variability observed in ref. [2-7], supporting that the conduction and switching mechanisms in filamentary and non-filamentary RRAMs are different. In filamentary RRAM, conduction at LRS is metallic-like, with electrons hopping through a filament formed by oxygen vacancies, leading to very small variability and RTN signals [4-5]. At HRS, its resistance is controlled by the critical constriction region where the least number of defects exist. Movement and trapping/detrapping of individual defect within and near the constriction has significant impact on the current conduction, hence the much larger variability and larger RTN amplitude and its much wider distribution. In contrast, the similarity between RTN distributions at LRS and HRS in non-filamentary RRAM suggests a similar conduction mechanism. The slightly larger RTN amplitude at HRS can be attributed to the slightly larger impact by trapping/detrapping since the defect profile is narrower in TiO_2 at HRS. The resistance variability and RTN amplitude at HRS is much smaller and tightly distributed than in filamentary RRAM, supporting that the impact of individual defect is significantly reduced due to the uniform defect distribution in a-VMCO device.

3.3 Degradation in stressed aVMCO RRAM

A typical current-time characteristics during the negative CVS is shown in **Fig. 5a&b**, where V_{stress} is applied on a fresh device. The device exhibits a two-stage cell degradation process. The CVS current is stable in the 1st stage, and there is a large current fluctuation in the 2nd stage, before the device reaches the final failure. As shown in the inset of **Fig. 5a&b**, the stress induced CVS current fluctuation can be as large as several times of the initial current, which does not exist in the fresh device. This is a strong indication of stress-induced defect.

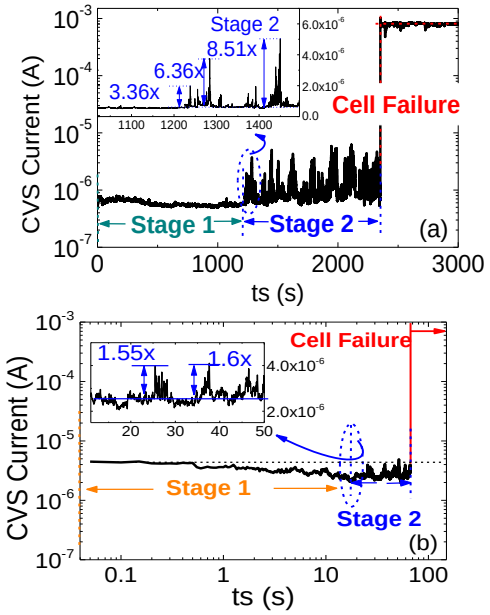

Fig. 5Typical I-t characteristics in a-VMCO RRAM. (a) Negative CVS (Vstress=-3.5V) is performed on a fresh device at LRS. (b) Positive CVS (Vstress= +6.6V) is performed on an unstressed device at HRS. The inset is the zoom-in of I-t when large fluctuations start to occur. Local current fluctuation of 50% is used as a criterion to define the onset of the 2nd stage.

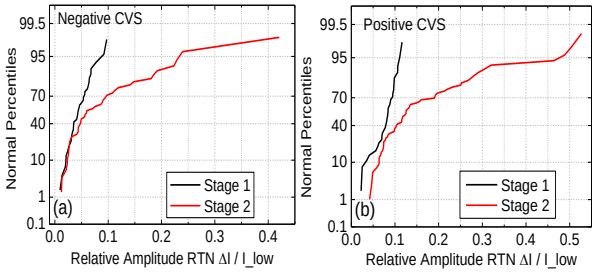

Fig. 6 CDF plot of the relative RTN amplitude distribution during the 1st and 2nd stage of (a) Negative and (b) Positive CVS.

This speculation is supported in **Fig. 6a&b**, where the CDF distributions of RTN amplitude exhibit long tails at large RTN amplitude in the 2nd stage, similar to that in the filamentary devices at HRS shown in **Fig. 4b**, indicating formation of filamentary percolation conduction path. There also exist small RTN amplitudes overlapping with that in the 1st stage.

3.4 Generated defects and percolation path

In order to provide direct experimental evidence to confirm the percolation current path formation in the 2nd stage during CVS, induced by defect generation as we speculated, defect locations are extracted from the small RTNs in the 1st stage and from the large RTNs in the 2nd

stage, respectively, during the positive CVS as shown in Fig. 7a, and the negative CVS as shown in Fig. 7b.

During the positive CVS, the a-VMCO device is reset at HRS, i.e. the off state. The profile of the defects extracted from the small RTNs in the 1st stage is represented by the orange rectangle in the background of Fig. 7a. Since there is a wide defect-'less' region near the IL at HRS, there is no percolation current path formed across the stack in this stage. During the 2nd stage, however, the defects extracted from the large RTNs show a different profile, which not only overlaps with that in the 1st stage, but also approaches the IL region across the TiO2 layer. Before the final failure occurs, the complete percolation path is expected to be formed across the entire stack and leads to the hard breakdown. This suggests that the 'defect-less' region in a-Si is the last stronghold of the dielectric stack before the device's final failure. Similar observations can be found for negative CVS at the on state (LRS) as shown in Fog. 7b.

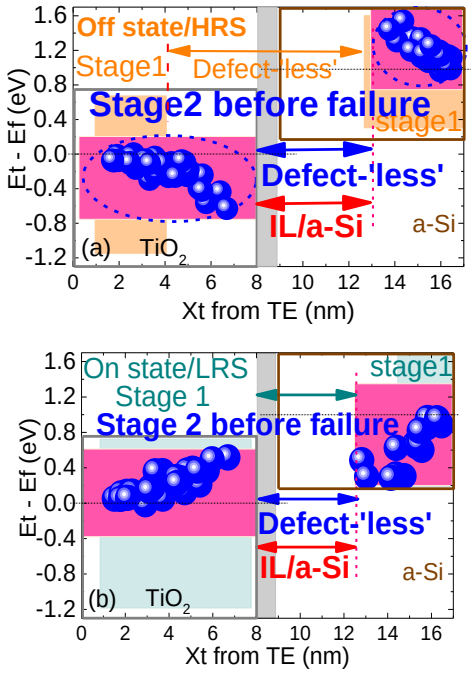

Fig. 7 Percolation path formation by defects generation in the 2nd stage of (a) positive and (b) negative CVS, in addition to the pre-existing defects observed during the 1st stage.

Conclusions

The switching, degradation and failure of amorphous-Si/ TiO2 based non-filamentary a-VMCO RRAM devices have been investigated in this work based on the random-telegraph-noise technique. The non-filamentary switching mechanism has been identified. It is found that the switching between the low and high resistance states are correlated with the profile modulation of pre-existing defects in the 'defect-less' region near the a-Si/TiO2 interface, and the non-filamentary switching leads to much smaller read instability at HRS than that in the filamentary RRAM devices. Defect generation induced percolation path formation is experimentally observed and correlated with the larger RTN amplitude and wide distribution in the stressed device.

Acknowledgments

This work was supported by the Engineering and Physical Science Research Council of UK under the grant no. EP/M006727/1. The authors would like to thank colleagues at IMEC, Belgium, for supply of test samples used in this work and fruitful discussions.

References

[1] Wong et al, IEEE proc., 2012.
[2] Govoreanu et al, IEDM, 2011.
[3] Govoreanu, et al, VLSI Symp. Tech. Dig., 2015
[4] Degraeve et al, VLSI, 2012.
[5] Chai, et al, VLSI Symp. Tech. Dig., 2016
[6]Ma, et al, IEDM 2016
[7] Chai, et al, IEEE, TED, 2017
[8] Kirton et al, Advances in Physics, 1989.
[9] Chang et al, IEDM 2008.